

Effects of sheds and cemented joints on seismic modelling of cylindrical porcelain electrical equipment in substations

Sheng Li*¹, Hing-Ho Tsang², Yongfeng Cheng¹ and Zhicheng Lu¹

¹China Electric Power Research Institute, Beijing, China

²Department of Civil and Construction Engineering, Swinburne University of Technology, Melbourne, Australia

(Received July 7, 2015, Revised November 1, 2016, Accepted November 7, 2016)

Abstract. Earthquake resilience of substations is essential for reliable and sustainable service of electrical grids. The majority of substation equipment consists of cylindrical porcelain components, which are vulnerable to earthquake shakings due to the brittleness of porcelain material. Failure of porcelain equipment has been repeatedly observed in recent earthquakes. Hence, proper seismic modelling of porcelain equipment is important for various limit state checks in both product manufacturing stage and detailed substation design stage. Sheds on porcelain core and cemented joint between porcelain component and metal cap have significant effects on the dynamic properties of the equipment, however, such effects have not been adequately parameterized in existing design guidelines. This paper addresses this critical issue by developing a method for taking these two effects into account in seismic modelling based on numerical and analytical approaches. Equations for estimating the effects of sheds and cemented joint on flexural stiffness are derived, respectively, by regression analyses based on the results of 12 pieces of full-scale equipment in 500kV class or higher. The proposed modelling technique has further been validated by shaking table tests.

Keywords: porcelain electrical equipment; seismic modelling; shed; cemented joint; shaking table test

1. Introduction

A wide variety of cylindrical porcelain electrical equipment, such as post insulator, surge arrester and capacitor voltage transformer, is a major component of a substation. The column-like equipment is usually made of porcelain insulators or housings that are mounted on each other. Due to the brittle nature of porcelain, equipment made of porcelain is typically vulnerable to earthquake shakings. Post-earthquake field investigations of recent earthquakes have shown that failure of insulators has a brittle fracture surface on porcelain component, and in many cases the failed insulators had fallen on the ground, for instance, 2008 Wenchuan Earthquake (Yu *et al.* 2008, Liu *et al.* 2010, Xie 2013) (as seen in Fig. 1), and 2013 Lushan Earthquake (You and Zhao 2013).

Modern electrical grids consist of substations in higher voltage classes. Nowadays, 500 kV or higher voltage class grids form the major electrical grids in many countries. The scale of electrical equipment in these substations is significantly larger than those in traditional substations. For example, a 220 kV surge arrester is 3-5 m in height and weighs nearly 0.5 ton, and a 500 kV surge arrester could be 5-8 m in height and weighs nearly 1 ton. For a surge arrester higher than 750 kV, it can reach a height of 10-13 m and as heavy as 5 ton. Hence, the earthquake-induced forces

on these types of equipment also increase dramatically. The vulnerable porcelain equipment might become the weakest link in a substation in an event of an earthquake. Hence, it is of utmost importance to enhance the reliability of the power grid by improving the seismic performance of porcelain equipment. A proper modelling tool is indeed indispensable for more accurate and robust analysis and design of such equipments.

Physical testing, such as shaking table test, is a desirable method for checking the seismic safety of electrical equipments in substations (IEEE Standard 693 2005, Fahad 2013, Takhirov *et al.* 2004, Filiatrault and Matt 2005). However, for equipments in 500kV class or higher, full-scale shaking table test is not commonly adopted partly due to the high cost of the specimen, and suitable testing facilities are not readily available everywhere. Hence, numerical simulation is a more popular way for studying the seismic performance at both equipment level and system level.

3D solid finite element and equivalent beam element can be adopted for modelling porcelain equipments. Owing to the irregular shape of porcelain component and the adhesive joint between porcelain and metal cap, the construction of a 3D finite element model is a complex and time consuming task. Alternatively, equivalent beam model is more often adopted in seismic analysis. Paolacci and Giannini (2009) have carried out seismic fragility analysis of a porcelain disconnect switch. 3D solid element model was built for a single insulator, in which more than 28,000 3D solid elements were employed and the adhesive joint was represented by equivalent elastic material. Due to the complexity in 3D solid element modelling, it is noteworthy

*Corresponding author
E-mail: lisheng@epri.sgcc.com.cn



Fig. 1 Failure of cylindrical porcelain equipment in a 220kV substation after 2008 Wenchuan Earthquake (Xie 2013)

that beam model was adopted in seismic analysis instead.

Two kinds of beam models, namely, uniform beam method and multi-section beam method, can be employed to model cylindrical equipments. For uniform beam method, flexural stiffness of the beam is a key factor that affects the accuracy of the model. Song *et al.* (2007), Whittaker *et al.* (2007), Gilani (2000), Kiureghian *et al.* (2001), Dastous (2007) and IEEE Standard 1527 (2006) have simplified the equipment to a single-degree-of-freedom (SDOF) oscillator in analysis. Mohammadi *et al.* (2012, 2013) has built a uniform beam with an additional concentrated mass at the top to represent an equipment. The stiffness of the SDOF system or uniform beam is determined from the fundamental natural frequency of the equipment. Chinese code GB505566 (2010) recommends a simple formula for estimating the fundamental frequency of equipment, and a uniform beam model can be built based on the estimated frequency. Filiatrault and Stearns (2002, 2003) and Dastous *et al.* (2004) studied the seismic interaction between two generic equipments that were linked by flexible conductor through shaking table tests. The generic equipments employed in the test were represented by steel columns with uniform section.

Uniform beam method is an effective approach for examining the seismic response of porcelain equipment. However, it has neglected the actual characteristics of the equipment. Hence, multi-section beam method, which allows different section properties for different parts of the porcelain equipment, is a more desirable approach. However, the effects of sheds surrounding the porcelain core and cemented joints between porcelain component and metal cap become significant in the use of the multi-section beam method.

Sheds are a series of corrugations or concentric disc shapes forming the outer layer of a porcelain insulator. The shape is specially designed to maximise the surface path length for the leakage currents and to prevent flashovers. As sheds are also made of porcelain, the enlarged sections at certain locations may contribute to the flexural stiffness of the porcelain equipment. In Kong (2010), the diameter of porcelain core of the tested insulator is 4.7 inch (119 mm), whilst the equivalent diameter adopted in the model is 7.4 inch (189 mm) after considering the effects of sheds. The

effect of sheds on flexural rigidity has been illustrated by 3D finite element analysis (Fabrizio and Giannini 2009), but it has not yet been parameterized for beam element modelling. For porcelain equipment with larger diameter, the dimension and thickness of sheds are usually small comparing to that of porcelain core, and the effects of sheds on the stiffness may become less significant. However, the mechanism of the effect has not been systematically investigated.

The rotational stiffness of cemented connection between porcelain and metal cap is unique, and has great influences on the overall stiffness of equipment. Various researchers have pointed out that such effect should be properly taken into account in numerical modelling. Gilani *et al.* (1999) and Whittaker *et al.* (2004) carried out shaking table test for porcelain bushing and studied the rotational response behaviour between porcelain component and metal flange by rocking radian measurement. It was found that excessive slip at the connection would cause oil leakage, which could lead to seismic failure of the bushing. Kong (2010) and Fabrizio and Giannini (2009) developed a beam model for simulating a post insulator and employed a link element for modelling the connection between porcelain component and metal cap, in which the stiffness of link element was derived from static push and pull test. However, this experiment based method is not applicable when such test has not been done. On the other hand, Eq. (1) has been adopted in both the Japanese code JEAG5003 (2010) and Chinese code GB50260 (2013) for estimating rotational stiffness

$$K_c = 6.54 \times 10^7 \frac{D_c h_c^2}{t_e} \quad (1)$$

in which D_c , h_c and t_e are the dimensions (in m) at the connection (refer Fig. 7) and K_c is the rotation stiffness of the connection (in N.m/rad). However, the equation form and the coefficients should be dependent on the scale of the equipment. The coefficient of 6.54 was obtained mainly from regression analysis of test results based on equipments of voltage class lower than 500 kV. The validity of this equation for higher voltage class equipments is questionable.

This paper focuses on the seismic modelling of large cylindrical porcelain electrical equipments, which are prevailing in power grids of 500 kV class or higher. Porcelain sheds stiffness factor and cement connection stiffness factor are introduced to represent the flexural rigidity of porcelain equipments, which forms a critical part of a practical method for modelling porcelain equipment in seismic analysis. In the last section of this paper, the accuracy of the proposed modelling method will be validated by shaking table tests.

2. Dynamic characteristics of cylindrical porcelain electrical equipments

Mass distribution, flexural stiffness and damping are three main aspects that determine the dynamic properties of a structure. Mass distribution of equipments can be obtained

Table 1 Basic parameters and dynamic properties of the high voltage class cylindrical porcelain equipments

Item No.	1	2	3	4	5	6	
Type *	SA	SA	PI	PI	SA	SA	
Basic parameters	Voltage class	500kV	750kV	500kV	750kV	>750kV	>750kV
	Mass (kg)	1100	3129	683	1531	7150	9776
	Height (m)	5.63	8.09	4.4	6.8	11.8	11.8
	No. of units	3	4	3	3	5	4
Dynamic properties	f_1 (Hz)	2.97	1.8	6.7	3.27	1.4	2.08
	damping ratio (%)	1.2	1.56	1.76	2.07	1.73	2.47
Item No.	7	8	9	10	11	12	
Type *	SA	CVT	CVT	CVT	SA	CVT	
Basic parameters	Voltage class	>750kV	>750kV	>750kV	>750kV	>750kV	>750kV
	Mass (kg)	6916	4691	2257	6751	5106	5791
	Height (m)	10.6	9.41	6.02	10.6	11.8	10.58
	No. of units	5	4	4	5	5	5
Dynamic properties	f_1 (Hz)	1.71	2.08	2.5	1.83	1.59	1.73
	damping ratio (%)	1.73	1.6	NA	NA	NA	NA

*SA: Surge Arrester; PI: Post Insulator; CVT: Capacitor Voltage Transformer

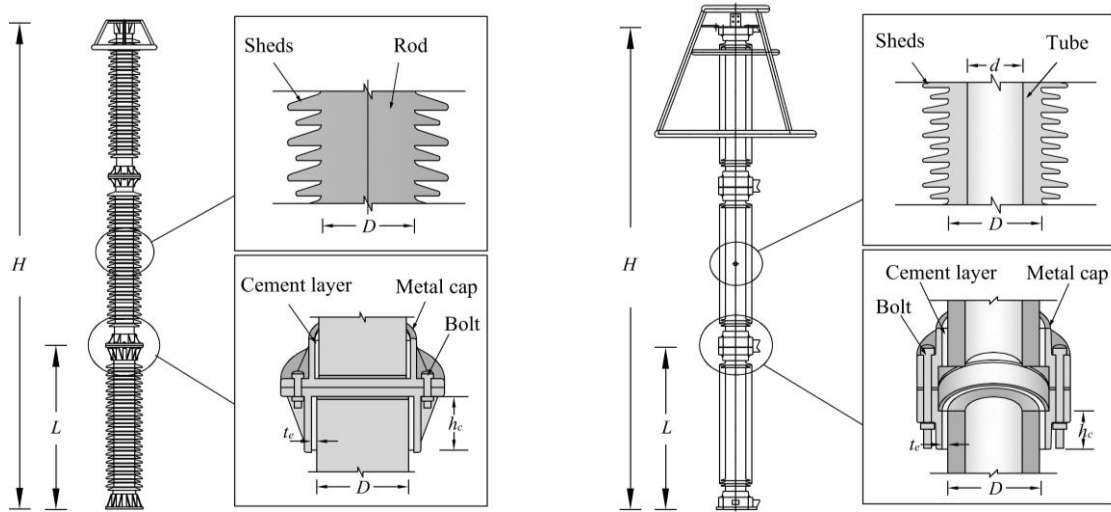


Fig. 2 Typical sections of (left) solid core post insulator (PI) and (right) surge arrester (SA)

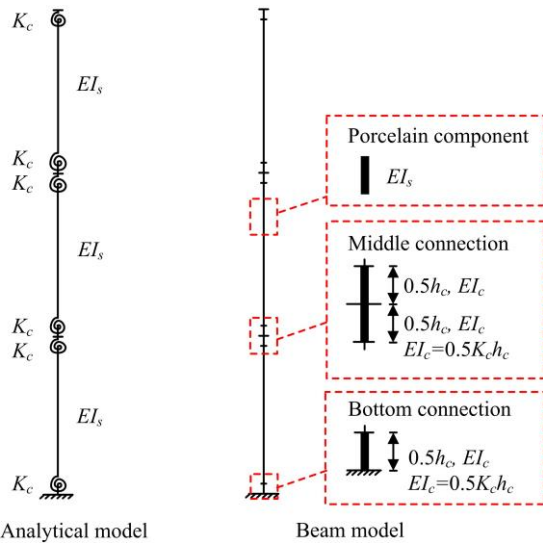


Fig. 3 Proposed analytical model and the equivalent beam model of a typical porcelain equipment

from product specification provided by manufacturers. For damping ratio, results from shaking table tests of 12 pieces of typical porcelain equipment in high voltage class substations (500 kV or higher), including surge arrester (SA), post insulator (PI) and capacitor voltage transformer (CVT), have been summarised in Table 1. White noise input ground motions with acceleration amplitude of 0.05 g were applied in the test. It can be found that the damping ratio of these porcelain equipments falls in the range of 1.2% to 2.5% for such shaking level. The damping may increase when seismic response increases, but for elastic analysis that is commonly adopted for brittle porcelain equipment, a damping value of 1.5% or 2% is considered conservative for seismic safety check. When mass distribution and damping are found, flexural rigidity becomes the remaining challenge in seismic modelling.

Fig. 2 shows the key structural elements and typical sections of a solid core post insulator and a surge arrester

Table 2 Deflections obtained from 3D finite element modelling and the proposed sheds coefficient λ_s

Item No.	D_c (m)	d_c (m)	Deflection (mm)		λ_s
			Without sheds	With sheds	
1	0.239	0.145	5.18	4.63	1.12
2	0.355	0.270	1.27	1.17	1.08
3	0.215	0	3.82	3.30	1.16
4	0.265	0	7.36	6.53	1.13
5	0.600	0.500	0.89	0.84	1.06
6	0.700	0.600	1.36	1.28	1.06
7	0.510	0.400	0.94	0.89	1.06
8	0.443	0.340	2.08	1.94	1.07

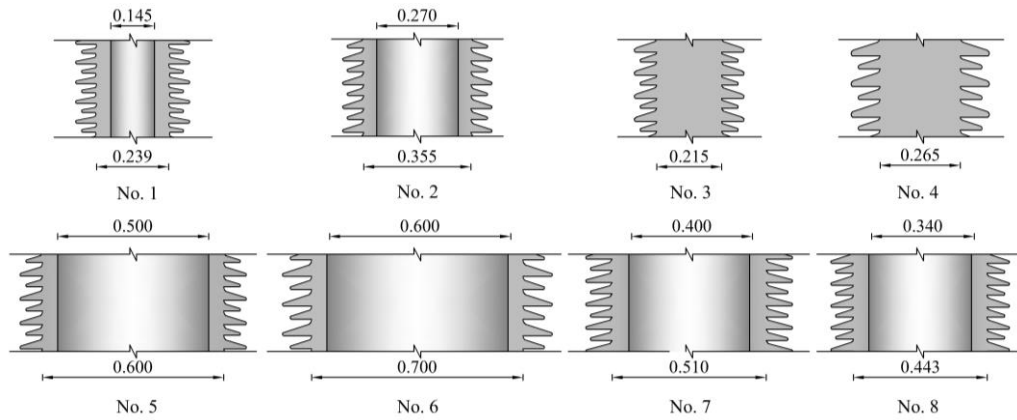


Fig. 4 Longitudinal sections of porcelain components and dimensions of core of equipment item No. 1 - 8 (unit: m)

with hollow core housing. These two pieces of equipment have common structural characteristics: (1) the main body of the equipment is made of porcelain tube or rod with sheds, as annotated in Fig. 2; (2) the porcelain component is connected through metal caps at both ends with bolted flange connection, as annotated in Fig. 2. The flexural rigidity of porcelain core with sheds and rotational stiffness at connection are the two determinants of the equipment's flexural stiffness.

The cross-section of porcelain component with sheds is complex and varies along the longitudinal axis. The flexural stiffness cannot be estimated conveniently which hinders the calculation of the dynamic properties of the equipment. In this study, EI_s is proposed as the effective section rigidity. The connection between porcelain component and metal cap typically consists of cementitious material. The rotational stiffness of the cemented joint is usually small, which would greatly affect the dynamic properties of equipment (Paolacci and Giannini 2009, Kong 2010, JEAG5003 2010, GB50260 2013). The parameter K_c has been used to represent the rotational stiffness at the connection. Hence, an analytical model and an equivalent beam model of a typical porcelain equipment can be constructed as in Fig. 3. The connection is represented by a rotational spring or a short beam with equivalent rotational stiffness. Assuming the length of the beam is $0.5h_c$, the flexural rigidity of the equivalent short beam is

$$EI_c = 0.5K_c h_c \quad (2)$$

3. Modelling flexural rigidity of sheds

Fig. 4 shows the longitudinal sections of the porcelain components of 8 pieces of equipment listed in Table 1 (Item No. 1-No. 8). As seen in the figure, the porcelain components are made of multiple layers of outer sheds and an inner rod or tube. The shape of outer sheds is complex and varies longitudinally, whilst inner core is uniform along the longitudinal direction. The cross section of rod is circular with diameter D , and the cross section of tube is a ring with inner diameter d and outer diameter D . The values of D and d are showed in Fig. 4.

The flexural rigidity of porcelain core can be calculated by Eq. (3) or Eq. (4)

$$EI_{rod} = (1/64)\pi D^4 E_p \quad (3)$$

$$EI_{tube} = (1/64)\pi(D^4 - d^4)E_p \quad (4)$$

The size and cross-section of sheds vary between products from different manufacturers. For insulator with larger diameter D , the dimension of sheds also increases, but the rate of increase is not linear. As seen in Fig. 4, the ratio of outer diameter between equipment No. 6 and equipment No. 3 is nearly 3, but the ratio of sheds' dimensions is around 2. As it is hard to determine the contribution of sheds to the stiffness of the component directly, 3D finite element modelling was adopted to study how sheds affect the overall flexural rigidity.

By introducing a sheds coefficient λ_s , the flexural rigidity of the cross section can be written as Eq. (5)

$$EI_s = \lambda_s EI_{core} \quad (5)$$

Take the 500 kV surge arrester housing as an example: as seen in Fig. 5(a), porcelain housing with sheds and cylinder without sheds have been modelled by 3D solid elements. For the cylinder model, outer diameter is D and inner diameter is d , which is the same as the main body of porcelain housing. A lateral load is acted at one end, whilst the other end is fixed. The deflections of the housing model and the cylindrical model have been computed, as seen in Fig. 5(b). The deflection of the porcelain housing with sheds is 4.63 mm, and the deflection of the cylindrical model is 5.18 mm. For the two cantilever structures that were analysed, the deflection ratio reflects the ratio of flexural rigidity, so the sheds coefficient λ_s for the 500 kV surge arrester housing is $5.18/4.63=1.12$.

Adopting the same procedure to the other 7 insulators or housings, values of λ_s are summarised in Table 2. Regression analysis for the relationship between D_c and λ_s is shown in Fig. 6.

The relationship between D_c and λ_s is proposed as follows

$$\lambda_s = 1.045 + 5 \times 10^{-3} D_c^{-2} \quad \text{where } 0.215m < D_c < 0.7m \quad (6)$$

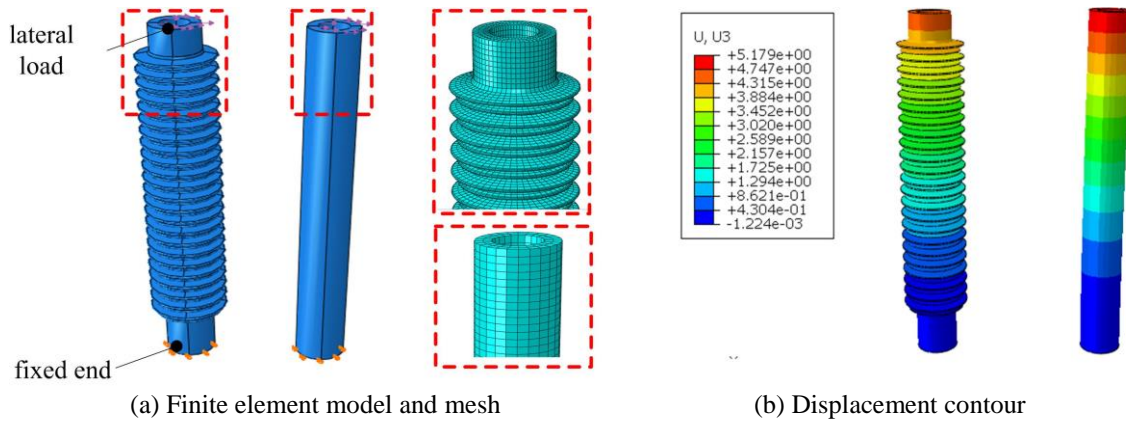


Fig. 5 The 3D finite element model of porcelain housing, with and without sheds, adopted in this study

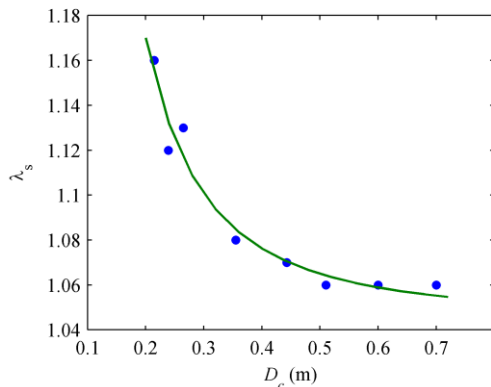


Fig. 6 Sheds coefficient λ_s : Regression analysis of results obtained from 3D finite element modelling

The r statistic for the regression above is 0.97. The equation above is supposedly applicable to the stated range of D_c only. Predictions of λ_s for equipment size out of the range are not expected.

4. Modelling rotational stiffness of cemented joints

The connection between porcelain components contains two main parts, namely, cemented connection between porcelain and metal cap, and bolted connection between two flanges. Fig. 7(a) shows the longitudinal section of cemented joint between porcelain component and metal cap. The thickness of the cement is t_e , height of the cement layer is h_c and diameter at connection is D_c . When the equipment is subjected to bending moment M , the porcelain rod or tube rotates by an angle θ , as shown in Fig. 7(b).

For the bolted connection, the bolts are usually pre-tensioned and no opening between the two faces is expected when the equipment is subjected to bending moment. The rotational stiffness of the bolted connection can be assumed infinitely large and has negligible effect on the overall rotational stiffness of equipment. Hence, the rotational stiffness Kc is mainly governed by the rotational stiffness of the cemented joint.

The rotational stiffness of the cemented connection, K_c , can be expressed using Eq. (7)

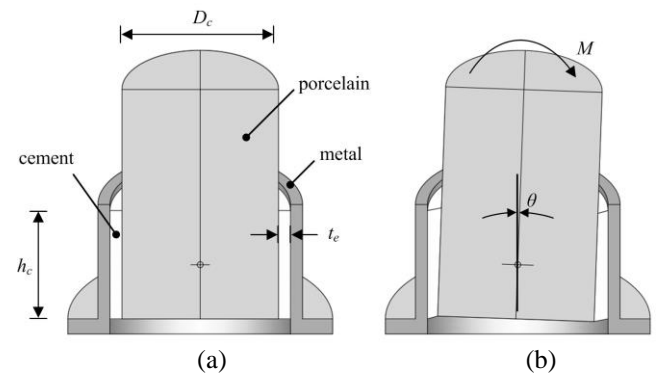


Fig. 7 Longitudinal section of cemented joint: (a) key dimensions for analytical modelling, and (b) definition of bending moment M and the corresponding rotation θ

$$K_c = \frac{M}{\theta} \quad (7)$$

The exact mechanics of the rotational stiffness K_c is complex, which involves nonlinear mechanical properties of the cementitious material and the mechanics at the contact interfaces. A practical method is proposed as follows for estimating the rotational stiffness of the cemented joint, which could be useful for design and engineering applications. The proposed method is developed based on a 2D analytical model of the cemented joint described as follows.

In the cemented connection, external bending moment M induces axial and shear stress in the cement layer. Hence, in the analytical model, M is equivalent to the sum of the moment provided by axial resistance (M_1) and the moment provided by shear resistance (M_2) of the cement layer, which can be expressed using Eq. (8)

$$M = M_1 + M_2 \quad (8)$$

Similarly, the flexural stiffness at the connection can be expressed using Eq. (9)

$$K_c = K_{c1} + K_{c2} \quad (9)$$

in which K_{c1} is the flexural stiffness associated to axial deformation and K_{c2} associated to shear deformation.

In the analytical model, the flexural stiffness K_c can be represented by two sets of uniformly distributed springs, including a pair of spring arrays with axial stiffness k_i and another pair of spring arrays with shear stiffness k_j , as showed in Fig. 8(a) and Fig. 8(b) respectively. The rotation centre of porcelain core under bending moment can be assumed at mid-height of the cement layer.

Given a certain amount of displacement, the reaction force is inversely proportional to the length of the spring. Hence, both k_i and k_j are inversely proportional to t_e . As the analytical model is a 2D simplification of a 3D cylindrical connection, both k_i and k_j are proportional to D_c . As shown in Fig. 9(a), the spring array for axial stress on each side is further simplified to a spring with axial stiffness k_c (for compression) and another spring with axial stiffness k_t (for tension). As shown in Fig. 9(b), the spring array for shear stress on each side is further simplified to two springs with stiffness k_s . Then, k_c , k_t or k_s is proportional to the length of cement layer h_c , which can be expressed using Eqs. (10)-(12)

$$k_c = \lambda_{1c} \frac{D_c h_c}{t_e} \quad (10)$$

$$k_t = \lambda_{1t} \frac{D_c h_c}{t_e} \quad (11)$$

$$k_s = \lambda_2 \frac{D_c h_c}{t_e} \quad (12)$$

In Fig. 9, concentrated springs should produce the same moment as the linearly distributed springs in Fig. 8. Hence, a spring in Fig. 9 should be placed at the position of

concentrated force resulted by half of the axial springs on each side (as shown in Fig. 8). In Fig. 9(a), considering the triangular distribution of displacement for axial springs under a rotation θ , the moment arm of concentrated spring in Fig. 9(a) should be $(1/3)h_c$, then the separation of the two springs (on each side) is $(2/3)h_c$. In Fig. 9(b), considering the rectangular distribution of shear displacement, the moment arm of concentrated spring in Fig. 9(b) should be $(1/4)h_c$, then the separation of the two springs is $0.5h_c$

In Fig. 9(a), assuming the deformation of spring is Δ_1 , the reaction forces of the springs are

$$F_{1c} = k_c \Delta_1 \quad (13)$$

$$F_{1t} = k_t \Delta_1 \quad (14)$$

The flexural resistance can be expressed using Eq. (15)

$$M_1 = (2/3)h_c (F_{1t} + F_{1c}) \quad (15)$$

By substituting Eqs. (13) and (14) into (15), it becomes

$$M_1 = (2/3)h_c (k_t + k_c) \Delta_1 \quad (16)$$

Based on the geometry as shown in Fig. 9(a), the relationship between θ and Δ is

$$\theta = \frac{3\Delta_1}{h_c} \quad (17)$$

By substituting Eq. (17) into Eq. (16), the moment produced by axial stress resistance becomes

$$M_1 = (2/9)(k_t + k_c)h_c^2 \theta \quad (18)$$

Referring to Eq. (7), the flexural stiffness associated to

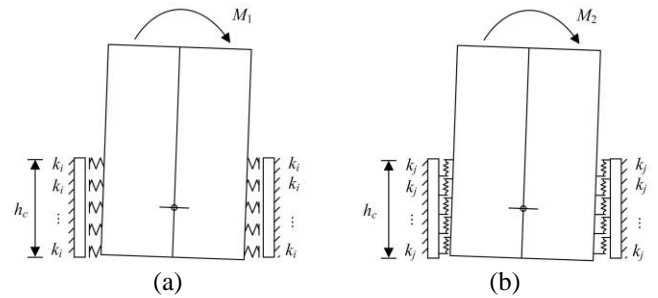


Fig. 8 Proposed analytical model of the cemented joint with distributed springs representing (a) axial stiffness and (b) shear stiffness of the cement layer

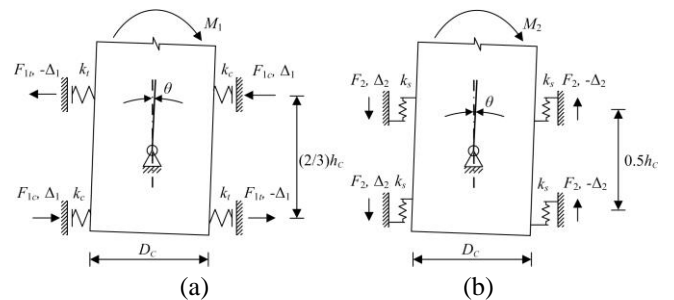


Fig. 9 Proposed analytical model of the cemented joint with concentrated springs representing (a) axial stiffness and (b) shear stiffness of the cement layer

axial deformation can be expressed as

$$K_{c1} = (2/9)(k_t + k_c)h_c^2 \quad (19)$$

Then, by substituting the expression of k_c and k_t into the expression of K_{c1} , it becomes

$$K_{c1} = \lambda_1 \frac{D_c h_c^3}{t_e} \quad (20)$$

in which $\lambda_1 = (2/9)(\lambda_{1c} + \lambda_{1t})$.

Based on Fig. 9(b), assuming that the deformation of spring is Δ_2 , the reaction force of the spring is

$$F_2 = k_s \Delta_2 \quad (21)$$

The contribution to flexural resistance can be expressed using Eq. (22)

$$M_2 = 2F_2 D_c \quad (22)$$

By substituting Eq. (21) into (22), it becomes

$$M_2 = 2k_s \Delta_2 D_c \quad (23)$$

Based on the geometry as shown in Fig. 9(b), the relationship between θ and Δ is

$$\theta = \frac{2\Delta_2}{D_c} \quad (24)$$

By substituting Eq. (24) into Eq. (23), the moment produced by shear resistance becomes

$$M_2 = k_s D_c^2 \theta \quad (25)$$

According to Eqs. (7)-(9), K_{c2} can be expressed as

$$K_{c2} = k_s D_c^2 \quad (26)$$

Then substituting the expression of k_s , i.e., Eq. (12), into Eq. (26), K_{c2} becomes

$$K_{c2} = \lambda_2 \frac{h_c D_c^3}{t_e} \quad (27)$$

By substituting Eqs. (20) and (27) into Eq. (9), the flexural stiffness at the connection can be expressed as

$$K_c = (\lambda_1 h_c^2 + \lambda_2 D_c^2) \frac{D_c h_c}{t_e} \quad (28)$$

Through this analytical analysis, it is found that K_c is proportional to $D_c h_c / t_e$ and $(\lambda_1 h_c^2 + \lambda_2 D_c^2)$. The factors λ_1 and λ_2 are related to properties of the cement material, porcelain-cement contact interfaces and cement-metal contact interfaces. The expressions of λ_1 and λ_2 are highly nonlinear and can be obtained individually using an empirical approach. Alternatively, a more convenient approach is to take the factor $(\lambda_1 h_c^2 + \lambda_2 D_c^2)$ as a whole and calibrate it using experimental data, which is considered appropriate for engineering application. Hence, let

$$\lambda_c = \lambda_1 h_c^2 + \lambda_2 D_c^2 \quad (29)$$

Then, K_c can be expressed as

$$K_c = \lambda_c \frac{D_c h_c}{t_e} \quad (30)$$

in which λ_c can be defined as rotation stiffness factor of the connection.

Values of K_c have been found for the 12 pieces of equipment through calibration of the numerical model such that the computed fundamental natural frequency matches with that obtained from shaking table test. These values of K_c are listed in Table 3, along with the dimensions of the cemented joint at the bottom of the equipment. Values of λ_c have then been obtained by using Eq. (30). Based on regression analysis and sensitivity study, it is found that λ_c has the strongest correlation with h_c amongst other parameters, and the result is shown in Fig. 10.

The expression for the rotation stiffness factor λ_c obtained from regression analysis is

$$\lambda_c = 5.25 \times 10^7 h_c \quad \text{where } 0.075m < h_c < 0.35m \quad (31)$$

The r statistic for the regression above is 0.63. The expression of K_c becomes

$$K_c = 5.25 \times 10^7 \frac{D_c h_c^2}{t_e} \quad \text{where } 0.075m < h_c < 0.35m \quad (32)$$

An important finding is that the equation form for K_c as obtained independently from an analytical-empirical approach is consistent with the model that has been adopted in two design codes. It is noteworthy that the equations in the codes were developed for porcelain equipment of low voltage class, whilst the specimens investigated in this study are for 500 kV voltage class or higher. As the coefficient obtained in this study is smaller (5.25×10^7), this

Table 3 Key dimensions of the cemented joint and rotation stiffness factor λ_c

No.	D_c (m)	t_e (m)	h_c (m)	f (Hz)*	K_c (N.m)	$D_c h_c / t_e$ (m)	λ_c (N)
1	0.239	0.0075	0.09	2.97	1.23×10^7	2.87	4.29×10^6
2	0.355	0.011	0.15	1.8	6.37×10^7	4.84	1.32×10^7
3	0.215	0.0075	0.138	6.7	3.54×10^7	3.96	8.95×10^6
4	0.265	0.016	0.145	3.27	1.39×10^7	2.40	5.78×10^6
5	0.6	0.02	0.2	1.4	7.92×10^7	6	1.32×10^7
6	0.7	0.008	0.32	2.08	3.44×10^8	28	1.23×10^7
7	0.51	0.01	0.2	1.71	1.02×10^8	10.2	1.00×10^7
8	0.443	0.011	0.22	2.08	6.86×10^7	8.86	7.74×10^6
9	0.355	0.014	0.14	2.5	3.97×10^7	3.55	1.12×10^7
10	0.53	0.0125	0.28	1.83	2.28×10^8	11.87	1.92×10^7
11	0.6	0.015	0.2	1.59	6.88×10^7	8	8.60×10^6
12	0.5	0.0125	0.24	1.73	1.41×10^8	9.6	1.47×10^7

(*fundamental natural frequency of equipment obtained from shaking table test)

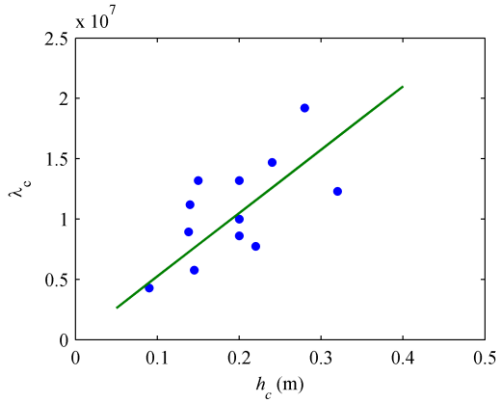


Fig. 10 Rotation stiffness factor λ_c : Regression analysis of data obtained from analytical modelling

indicates that the rotation stiffness of cemented joint is lower for larger scale equipment. On the other hand, effect of sheds is taken into account in the proposed model in this study, which is not well represented in the design codes.

The analysis of K_c and λ_c demonstrates the constituents of rotation stiffness of the cemented joint. When fundamental frequency of the equipment is available from product specification or test report, an accurate value of K_c and λ_c can be obtained by calibration using computational model. As testing result is usually unavailable, Eq. (32) can be used to estimate the rotation stiffness of the joint.

5. Validation

In this section, the accuracy and effectiveness of the proposed modelling method will be validated and demonstrated by comparing the analysis results with experimental results from shaking table tests.

5.1 Model parameters and FE modelling

Shaking table test set-up of a 500 kV porcelain surge arrester (Item No. 1 in Table 1) is shown in Fig. 11(a). This equipment contains 3 insulators with the same configuration. The mass, dimension and material parameters are listed in Table 4. Estimated values of flexural rigidity for porcelain component and connection have also been calculated using the proposed method. Beam model can then be built according to these parameters, as seen in Fig. 11(b). It is noted that the grading ring at the top is made of aluminium tube with small mass, which is considered as non-structural element.

5.2 Seismic response estimation

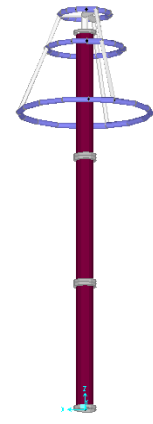
In the shaking table tests, accelerometers were installed at the top of each insulator of the specimen. Two strain gauges were symmetrically placed at the bottom of each porcelain component along the longitudinal direction. Input horizontal motions include one artificial wave and two recorded earthquake ground motions. In order to keep the

Table 4 Model parameters of insulators in a 500 kV porcelain surge arrester

Position of insulator unit		Top	Middle	Bottom	
Physical Parameters	Mass of main body, m (kg)	258	258	258	
	Concentrated mass at top, m_1 (kg)	82.6	51.5	44	
	Concentrated mass at bottom, m_2 (kg)	32	39.5	76.5	
	Length, L (m)	1.875	1.875	1.875	
	Porcelain Modulus, E (Pa)	9×10^{10}	9×10^{10}	9×10^{10}	
	Inner Diameter, d (m)	0.145	0.145	0.145	
	Outer Diameter, D_c (m)	0.239	0.239	0.239	
	Height of cement layer, h_c (m)	0.090	0.090	0.090	
	Thickness of cement layer, t_c (m)	7.5×10^{-3}	7.5×10^{-3}	7.5×10^{-3}	
	Rigidity Estimation	Sheds coefficient, λ_s	1.133	1.133	1.133
		Rotation stiffness factor, λ_c (N)	4.7×10^6	4.7×10^6	4.7×10^6
		Porcelain component's rigidity, EI_c (N.m ²)	1.41×10^7	1.41×10^7	1.41×10^7
Connection's rotation stiffness, K_c (N.m)		1.35×10^7	1.35×10^7	1.35×10^7	



(a)



(b)

Fig. 11 (a) Shaking table test set-up and (b) the finite element model for the 500 kV surge arrester (Item No. 1 in Table 1)

material behaviour in the elastic range, the values of peak ground acceleration (PGA) of the input ground motions were scaled to below 1.5 m/s^2 .

Fig. 12 shows the input seismic wave of the artificial ground motions (upper left), the results of horizontal acceleration responses at the top (upper right), the Fourier amplitude spectra of acceleration responses (lower left) and the stress responses at the bottom (lower right) from both shaking table test and numerical analysis. Fig. 13 and Fig. 14 show the results with the use of El Centro and Landers earthquake ground motions respectively. In the numerical

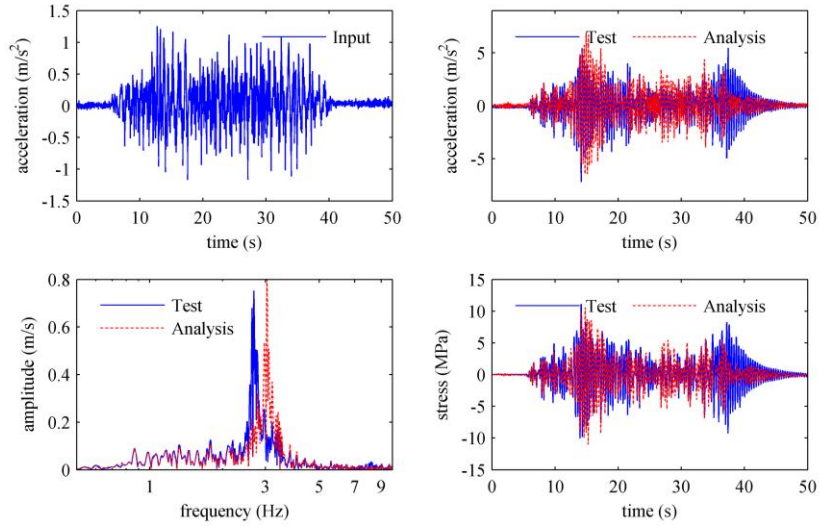


Fig. 12 Comparison between shaking table test results and numerical analysis results based on the artificial ground motions

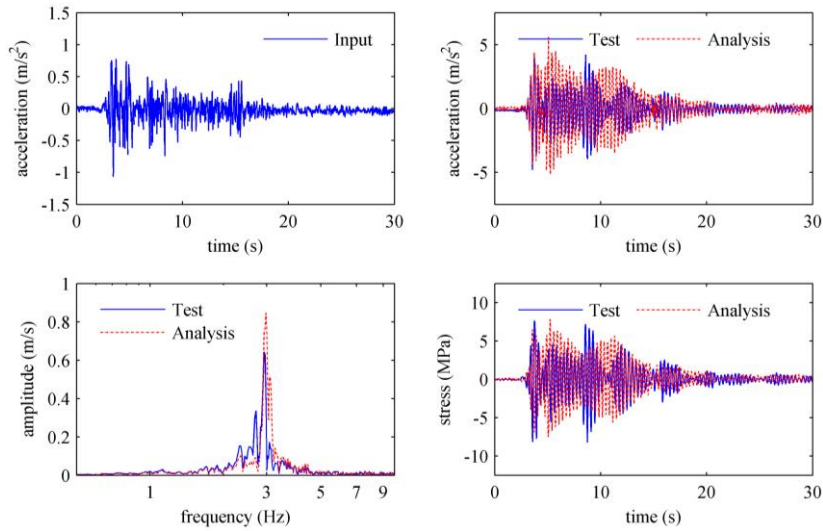


Fig. 13 Comparison between shaking table test results and numerical analysis results based on the 1940 El Centro earthquake ground motions

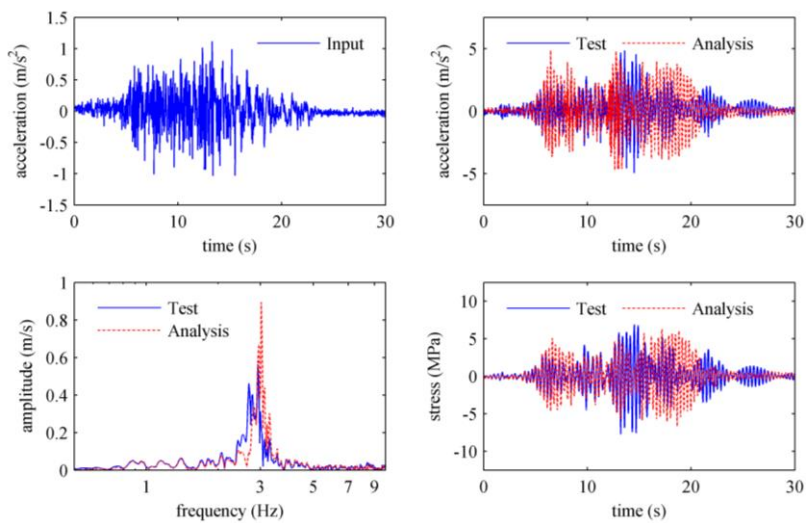


Fig. 14 Comparison between shaking table test results and numerical analysis results based on the 1992 Landers earthquake ground motions

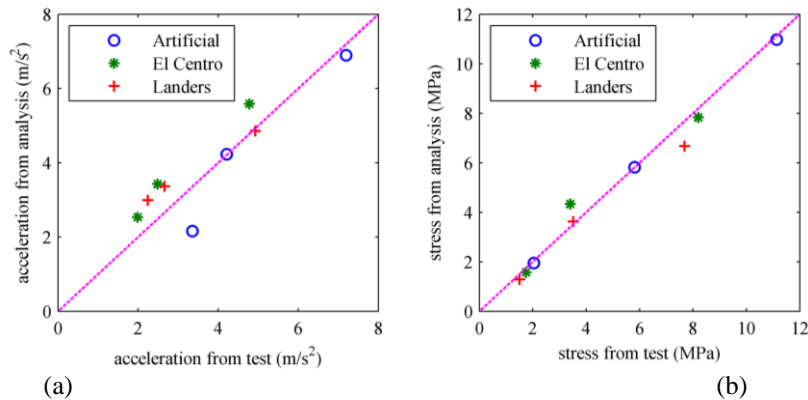


Fig. 15 Comparison of (a) acceleration and (b) stress responses resulted from shaking table tests and numerical analyses

Table 5 Comparison between results from shaking table tests and numerical analyses

Input motion (PGA)	Category	Acceleration (m/s ²)			Stress (MPa)		
		1	2	3	1	2	3
Artificial (0.13 g)	Shaking Table	7.19	4.21	3.36	2.04	5.81	11.13
	Numerical	6.90	4.23	2.16	1.95	5.82	10.98
El Centro (0.14 g)	Shaking Table	4.78	2.48	1.99	1.75	3.40	8.20
	Numerical	5.59	3.43	2.53	1.57	4.33	7.83
Landers (0.11 g)	Shaking Table	4.93	2.66	2.24	1.50	3.52	7.68
	Numerical	4.86	3.36	2.99	1.28	3.62	6.67

analysis, damping ratio was set as 1.5%. The stress responses of porcelain component were investigated because the failure of porcelain component is usually caused by excessive stress, and this controls the seismic safety of equipment directly.

The fundamental frequencies of the porcelain surge arrester as obtained from shaking table tests are 2.7 Hz, 2.9 Hz and 2.9 Hz as observed in the Fourier amplitude spectra, whilst the fundamental frequencies computed by numerical simulation is 3.0 Hz. This demonstrates a high level of accuracy of the proposed analytical model in terms of frequency estimation. Table 5 summarises the absolute maximum values of accelerations and stresses obtained from shaking table tests and numerical analyses.

Results are also plotted in Fig. 15 for close scrutiny. Each data point represents one insulator specimen. It can be seen that the response predictions based on the proposed analytical model have achieved a satisfactory level of accuracy and are unbiased. The average discrepancy amongst all the acceleration and stress response predictions is less than 15%, which is considered acceptable from the engineering perspective given the high level of variability in earthquake ground motions.

6. Conclusions

This study has pinpointed an important issue in the

seismic modelling of cylindrical porcelain electrical equipment in 500 kV voltage class or higher. Sheds on porcelain component and cemented joint between porcelain and metal cap have important influence on the dynamic properties of equipment, and should be taken into account in seismic modelling. By both numerical and analytical approaches, the effects of sheds on the flexural rigidity of porcelain core have been investigated and quantified, and can be taken into account by the proposed sheds coefficient λ_s . Cemented joint between porcelain component and metal cap has a negative effect on flexural rigidity of the equipment. The rotation stiffness of the joint can be estimated by the proposed equation of $5.25 \times 10^7 \times D_c h_c^2 / t_e$. The modelling technique developed in this study has been further validated by shaking table tests of 12 pieces of full-scale equipment. The proposed model can be adopted for numerical modelling of the key dynamic properties and seismic responses of porcelain equipment with an acceptable level of accuracy. This is also suitable for parameterisation in design standard and guidelines.

Acknowledgments

The research described in this paper was financially supported by the State Grid Corporation of China [GCB17201500063].

References

- Dastous, J.B. (2007), "Guidelines for seismic design of flexible buswork between substation equipment", *Earthq. Eng. Struct. Dyn.*, **36**(2), 191-208.
- Dastous, J.B., Filiatrault, A. and Pierre J.R. (2004), "Estimation of displacement at Interconnection points of substation equipment subjected to earthquakes", *IEEE T. Power Deliver.*, **19**(2), 618-627.
- Fahad, M. (2013), "Seismic evaluation and qualification of transformer bushings", Ph.D. dissertation, The State University of New York at Buffalo, Buffalo.
- Filiatrault, A. and Matt, H. (2005), "Experimental seismic response of high-voltage transformer-bushing systems", *Earthq. Spectra*, **21**(4), 1009-1025.
- Filiatrault, A. and Stearns, C. (2002), "Electrical substation

- equipment interaction-experimental flexible conductor studies”, University of California, San Diego, Structural Systems Research Project, Report No. SSRP-2002/09.
- Filiatrault, A. and Stearns, C. (2003), “An experimental study on the seismic response of electrical substation equipment interconnected by flexible conductors”, *Advancing Mitigation Technologies and Disaster Response for Lifeline Systems*, 667-676. California, August.
- GB50556 (2010), Code for aseismic design of electrical facilities in industrial plants, Beijing. (in Chinese)
- GB50260 (2013), Code for design of seismic of electrical installations, Beijing. (in Chinese)
- Gilani, A.S.J. (2000), “Seismic evaluation and analysis of 230 kV disconnect switches”, *PEER Report 2000/06*.
- Gilani, A.S., Whittaker, A.S., Fenves, G.L. and Fujisaki, E. (1999), “Seismic evaluation of 550 kV porcelain transformer bearings”, *PEER Report 1999/05*.
- IEEE Standard 693 (2005), IEEE Recommended Practice for Seismic Design of Substations, New York.
- IEEE Standard 1527 (2006), IEEE Recommended Practice for the Design of Flexible Bus work Located in Seismically Active Areas, New York.
- JEAG5003 (2010), Guidelines for Seismic Design of Electrical Equipment in Substation, Tokyo. (in Japanese)
- Kiureghian, A.D., Sackman, J.L. and Hong, K.J. (2001), “Seismic interaction in linearly connected electrical substation equipment”, *Earthq. Eng. Struct. Dyn.*, **30**(3), 327-347.
- Kiureghian, A.D., Hong, K.J. and Sackman, J.L. (2000), “Further studies on seismic interaction in interconnected electrical substation equipment”, *PEER Report 2000/01*.
- Kong, D. (2010), “Evaluation and protection of high voltage electrical equipment against severe shock and vibrations”, Ph.D. dissertation, The State University of New York at Buffalo, Buffalo.
- Liu R., Zhang M., Wu Y., Liu Y., Lin J. and Guo E. (2010), “Damage and failure study of Sicuan electric power grid in Wenchuan Earthquake”, *J. Basic Sci. Eng.*, **18**, 200-211. (in Chinese)
- Mohammadi, R.K., Akrami, V. and Nikfar, F. (2012), “Dynamic properties of substation support structures”, *J. Constr. Steel Res.*, **78**, 173-182.
- Mohammadi, R.K. (2013), “An improvement to seismic design of substation support structures”, *Struct. Eng. Mech.*, **45**(6), 821-835.
- Paolacci, F. and Giannini, R. (2009), “Seismic reliability assessment of a high-voltage disconnect switch using an effective fragility analysis”, *J. Earthq. Eng.*, **13**(2), 217-235.
- Song, J., Kiureghian, A.D. and Sackman, J.L. (2007), “Seismic interaction in electrical substation equipment connected by non-linear rigid bus conductors”, *Earthq. Eng. Struct. Dyn.*, **36**(2), 167-190.
- Takhirov, S.M., Fenves, G.L. and Fujisaki, E. (2004), “Seismic qualification and fragility testing of line break 550-kV disconnect switches”, *PEER Report 2004/08*.
- Whittaker, A.S., Fenves, G.L. and Gilani, A.S.J. (2007), “Seismic evaluation and analysis of high-voltage substation disconnect switches”, *Eng. Struct.*, **29**(12), 3538-3549.
- Whittaker, A.S., Fenves, G.L. and Gilani, A.S.J. (2004), “Earthquake performance of porcelain transformer bushings”, *Earthq. Spectra*, **20**(1), 205-223.
- Xie, Q. (2013), “Field Investigation on Damage of Substation Equipment in Wenchuan Earthquake, May 12, 2008”, Workshop on Electric System Earthquake Engineering, California, Berkeley.
- You, H. and Zhao, F. (2013), “M7.0 Earthquake in Lushan and Damage Cause Analysis of Power Facilities”, *Electric Power Construction*, **34**(8), 100-104. (in Chinese)
- Yu, Y., Li, G. and Li, P. (2008), “Investigation and analysis of electric equipment damage in sichuan power grid caused by Wenchuan earthquake”, *Power Syst. Technol.*, **32**(11), 1-6. (in Chinese)

KT